nature chemistry

Article

https://doi.org/10.1038/s41557-025-01916-7

Electrostatic atlas of non-covalent interactions built into metal–organic frameworks

Received: 3 October 2024

Accepted: 16 July 2025

Published online: 27 August 2025

Check for updates

Zhe Ji[1,5,7] ✉, Srijit Mukherjee[1,7], Jacopo Andreo[2], Anna Sinelshchikova[2], Francesca Peccati[3,4], Gonzalo Jiménez-Osés[3,4], Stefan Wuttke[2,6] ✉ & Steven G. Boxer[1] ✉

Non-covalent interactions are central to the organization of matter and molecular recognition processes, yet they are difficult to characterize. Here we devise a platform strategy to systematically build non-covalent interactions with selective chemical groups into precisely designed configurations by using metal–organic frameworks (MOFs) as the molecular scaffold. Using the vibrational Stark effect benchmarked against computer models, we find the electric field provides a unifying metric for quantifying diverse non-covalent interactions in MOFs and solvation environments. We synthesize and analyse spectroscopically a collection of non-covalent interactions using a nitrile probe within the MOF structure, and identify stabilizing fields as strong as −123 MV cm^{-1} produced additively by multiple hydrogen bonds, an unusual destabilizing field of +6 MV cm^{-1} between antiparallel dipoles, anomalous hydrogen-bond blueshifts as large as 34 cm^{-1} and unique solvation under nanoconfinement. This method for making and testing non-covalent interactions opens new avenues for exploring non-covalent interactions.

Non-covalent interactions are fundamental, ubiquitous forces that shape the properties and behaviours of molecules and their assemblies. These interactions can occur between any chemical groups that happen to get close enough, so there exists an enormous diversity of non-covalent interactions. While interactions such as hydrogen bonds (H bonds) are relatively strong and have well-defined and well-characterized properties, it is challenging to define most interactions, which are nonspecific and weak, even though their combination is often energetically substantial. Two primary experimental challenges must be overcome to assess individual non-covalent interactions: (1) how to systemically build individual non-covalent interactions between specific groups at precisely defined geometries without any direct covalent connection and (2) how to experimentally quantify these interactions from a physical perspective. We develop a general platform for placing selective chemical groups at defined positions and orientations using a metal–organic framework (MOF)[1–3], inspired by the molecular vise approach developed by Deng and co-workers[4–6]. In light of the fact that chemical groups that participate in non-covalent interactions can be mostly represented as charges and dipoles interacting with each other through their produced electric fields and the fact that electric fields oriented along reacting bond dipoles can reduce activation barriers and thereby promote chemical reactivity—an effect exemplified in enzyme electrostatic catalysis—we then measure the electric fields associated with our precisely designed non-covalent

[1]Department of Chemistry, Stanford University, Stanford, CA, USA. [2]Basque Center for Materials, Applications and Nanostructures (BCMaterials), Leioa, Spain. [3]Center for Cooperative Research in Biosciences (CIC bioGUNE), Basque Research and Technology Alliance (BRTA), Derio, Spain. [4]Ikerbasque, Basque Foundation for Science, Bilbao, Spain. [5]Present address: College of Chemistry and Molecular Engineering, Peking University, Beijing, China. [6]Present address: Academic Centre for Materials and Nanotechnology, AGH University of Krakow, Krakow, Poland. [7]These authors contributed equally: Zhe Ji, Srijit Mukherjee. ✉e-mail: jizhe@pku.edu.cn; swuttke@agh.edu.pl; sboxer@stanford.edu

https://doi.org/10.1038/s41557-025-01916-7

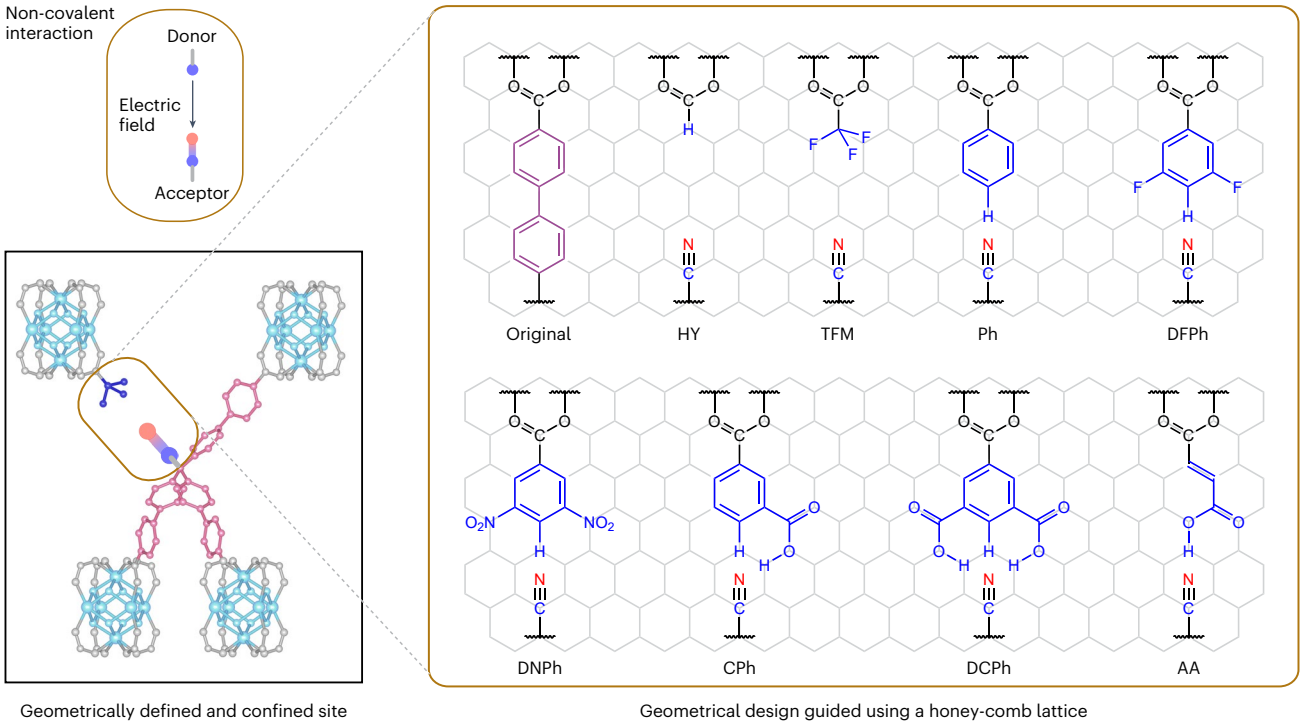

Fig. 1 | Electrostatic picture of non-covalent interactions and the molecular platform developed in this work. To study the electric fields produced by non-covalent interactions, we anchored a nitrile probe (field acceptor) against a series of field donors in a geometrically defined and confined site in a MOF. The field donor can be systematically varied by geometrical design, guided and visualized using a honey-comb lattice, resulting in an array of non-covalent interactions to be probed.

interactions using the vibrational Stark effect (VSE)[7–11] and characterize the electrostatic contribution to these interactions. Here, we refer to the chemical group that produces the electric field of interest as the electric field donor and the group that experiences the field as the acceptor, a nomenclature inspired by the commonly used H-bond donor/acceptor and here applied to non-covalent interactions in general.

Previous studies used vibrational probes to report the electric fields associated with diverse chemical environments including proteins[10–23], lipid membranes[24,25], solvation shells[11,26,27] and electrode-electrolyte interfaces[28,29]. Although these results have provided insights into specific interactions, especially those related to a substantial contribution of electrostatic pre-organization to the proficiency of enzymes, the chemical scope is limited because in solution and at interfaces the positioning of donor and acceptor typically cannot be controlled, and in biomolecules the range of electric field donors is largely constrained by bio-specificity evolved from nature. We overcome these limitations by using a rigid scaffold onto which an electric field probe (nitrile) is anchored in apposition to a series of field donors (Fig. 1). Specifically, a MOF is used to act as the structural backbone to hold the electric field donors and a nitrile acceptor as a probe in place. The permanent porosity of the MOF allows for the removal of solvent and isolation of the interrogated non-covalent interaction. Re-addition of solvent within this framework also provides a unique opportunity to examine solvation under nanoconfinement.

We chose a nitrile as the field probe because its vibrational frequencies lie in a part of the vibrational spectrum that is distinctly separate from background absorption and nitriles have been extensively studied for probing electric fields[12–17]. Using a calibration based on vibrational solvatochromism, perturbations to the nitrile vibrational frequency within the MOF scaffold in response to different apposing functionalities can be used to extract the electrostatic contribution to the interactions. The experimental results are then compared with computer simulations to interrogate and benchmark non-covalent interactions involving H bonds and the solvation effect under MOF nanoconfinement.

Results and discussion

Design and synthesis of MOFs holding field donor–acceptor pairs

We chose PCN-521 (ref. 30) as the MOF scaffold for positioning field donor–acceptor pairs (Fig. 2), the same MOF that Deng and co-workers developed for the molecular vise approach[4–6] owing to the ease of functionalization and the right size of the functionalization site. Single octahedral PCN-521 crystals (Supplementary Fig. 1) were synthesized by connecting $Zr_6O_4(OH)_4$ clusters (Fig. 2a, blue) with a tetrahedral organic linker, 4′,4″,4‴,4⁗-methanetetrayltetrabiphenyl-4-carboxylic acid (H_4L; Fig. 2a, green), into an extended network in a fluorite topology (Fig. 2b). The solvent inside the MOF pore was exchanged and removed by evacuation without structural collapse. The crystallinity and the composition were confirmed by powder X-ray diffraction (PXRD) (Supplementary Fig. 2) and digestion NMR spectroscopy (Supplementary Fig. 3), respectively.

To install a vibrational probe into the structure of PCN-521, we designed and synthesized a trigonal pyramidal organic linker, tris(4-carboxylbiphenyl)acetonitrile (H_3LCN; Fig. 2a, magenta, and Supplementary Figs. 4–11), which maintains three of the carboxylate groups in H_4L and bears a nitrile probe in the fourth position, facing into the pore. The incorporation of H_3LCN does not compromise the overall crystallinity of PCN-521, as evidenced by the unchanged PXRD pattern (Supplementary Fig. 12). We found that a 2:1 molar ratio of H_4L to H_3LCN in the reaction mixture led to a 4:1 molar ratio of H_4L to H_3LCN in the obtained PCN-521 crystals, as measured by digestion NMR spectroscopy (Supplementary Fig. 13 and Supplementary Table 1). The structural consequence of the linker substitution is that a fraction of the tetrahedral sites now has one biphenylene ligand replaced by a defined defect (Fig. 2b). On the opposite side, appended from the

https://doi.org/10.1038/s41557-025-01916-7

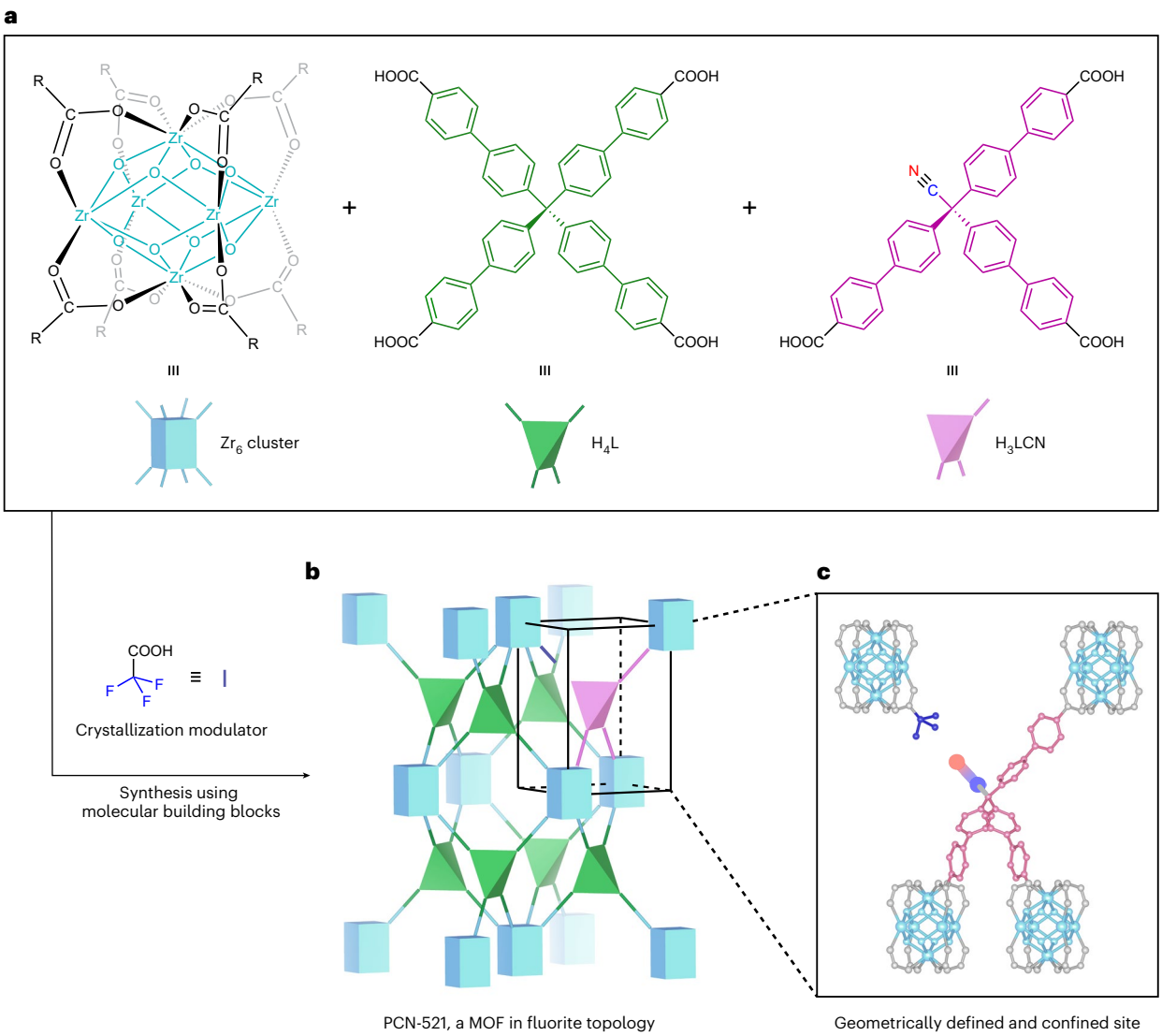

Fig. 2 | PCN-521, a MOF, acts as a molecular scaffold onto which field donors and acceptors are installed in fixed configurations. a, Molecular building blocks of the MOF. **b**, Connection of the metal cuboid (Zr_6 cluster) and the organic tetrahedron (H_4L) into a network in fluorite topology. **c**, Incorporation of the trigonal organic linker (H_3LCN) builds into the MOF crystals defective sites comprising a field donor ($-CF_3$) oriented towards a field acceptor (nitrile probe).

underconnected Zr cluster is the trifluoracetic acid modulator added in the reaction mixture, so the PCN-521 structure has abundant defect sites that comprise the $-CF_3$ group aligned towards the nitrile (Fig. 2c). After washing and evacuation, the intentionally created defect sites are free of solvent, hosting a specific non-covalent interaction between $-CF_3$ and the nitrile in isolation.

The molecular and modular nature of the MOF structure allows us to systematically replace the trifluoroacetic acid with a range of other carboxylate ligands (Fig. 1). The MOF crystals were soaked in methanol solutions of different carboxylic acids. The new carboxylic acid spontaneously substituted trifluoracetic acid, yielding a series of MOF variants we refer to as HY (a structure containing a hydrogen atom as the field donor), TFM (as synthesized, a trifluoromethyl donor), Ph (a phenyl donor), DFPh (a difluorophenyl donor), DNPh (a dinitrophenyl donor), CPh (a carboxylate phenyl donor), DCPh (a dicarboxylate phenyl donor) and AA (an acrylic acid donor), each bearing a unique field donor as shown in Fig. 1. The field donors were found to occupy 60–80% of the total open coordination sites as quantified by digestion NMR spectra (Supplementary Figs. 14–20 and Supplementary Table 1). Crystallinity of these MOF variants were confirmed by PXRD (Supplementary Fig. 12).

Electrostatic characterization of aprotic interactions via the vibrational Stark effect

Previous work has established that nitrile vibrational probes exhibit a linear vibrational Stark effect, vibrational frequency shifts in proportion to the magnitude of electric field, in aprotic environments[7–15] (Supplementary Texts 1–3). This does not extend to nitrile frequencies in protic (H-bonding) environments due to well-known anomalous blueshifts in frequency (Supplementary Text 4). Infrared absorption transition dipole moments of nitriles have been shown to exhibit linearity with the field in all environments[16]; however, this requires precise information on the absolute concentration of the nitrile, which is not applicable to the MOF powder samples studied here (Supplementary Text 4). Therefore, in this work we focus on using Raman scattering of bulk MOF samples to measure the vibrational frequency of nitrile to infer the magnitude of electric fields (note that intensity quantification under polarization is precluded by the strong birefringence exhibited by PCN-521 crystals; Supplementary Figs. 21 and 22 and Supplementary Text 5). The same measurement can be performed on any single-crystalline or polycrystalline sample that harbours specific interactions.

To calibrate the sensitivity of the nitrile's frequency shifts to electric fields (the Stark tuning rate, $\Delta\vec{\mu}$), we used triphenylacetonitrile

https://doi.org/10.1038/s41557-025-01916-7

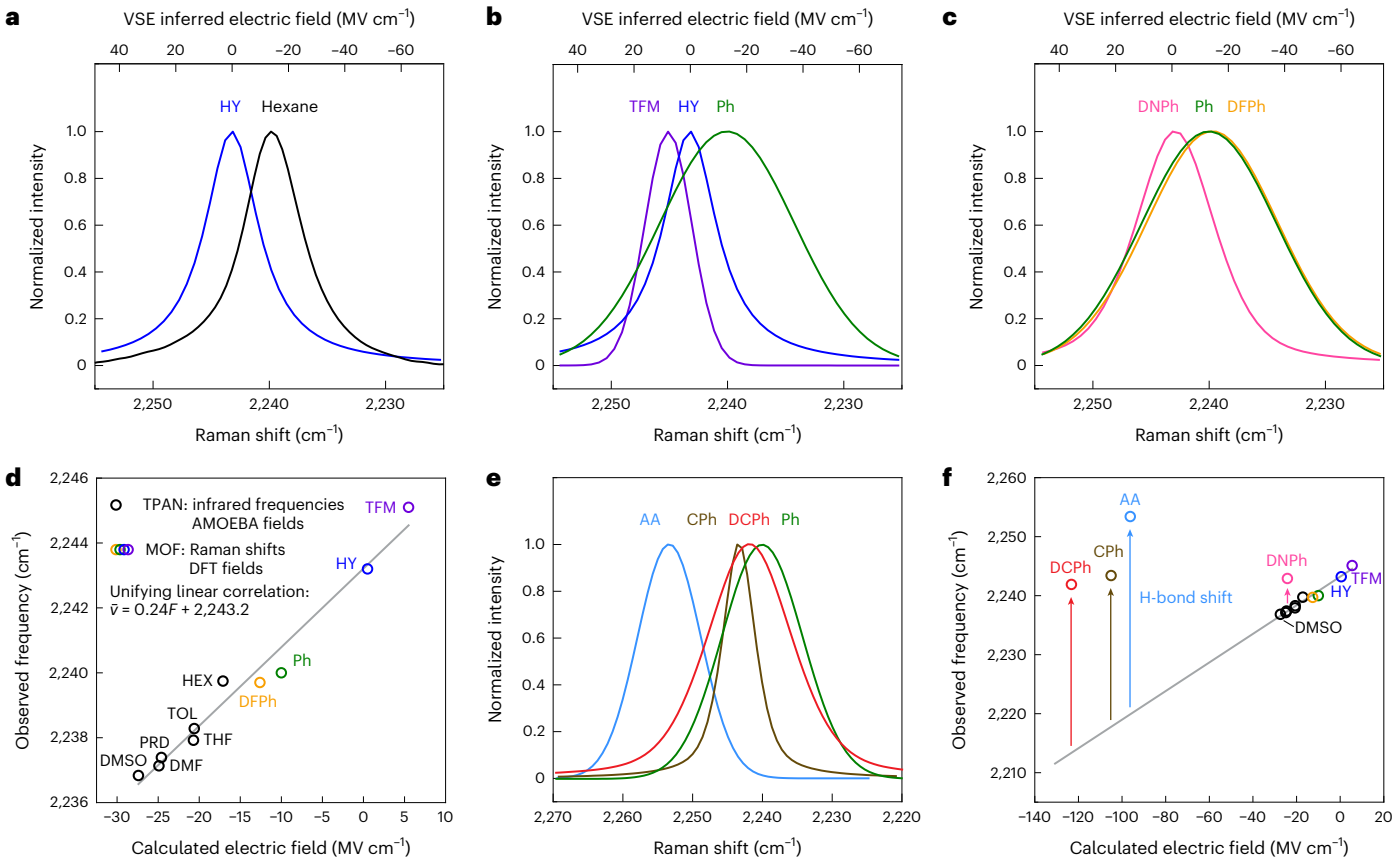

Fig. 3 | Raman spectroscopy and electric field calculation for the MOF structures. a, Fitted Raman spectrum for HY overlaid with the infrared spectrum of the TPAN model compound in hexanes (raw spectra shown in Supplementary Fig. 30 and fitting results listed in Supplementary Table 7). The top axis of the VSE inferred electric field derives from the linear correlation shown in **d**. **b**, Fitted Raman spectra for the HY, TFM and Ph variants. **c**, Fitted Raman spectra for the Ph, DFPh and DNPh variants. **d**, Field-frequency correlation plotted using (1) MOF variant data (coloured circles) with experimentally measured Raman shifts and DFT-calculated electric fields and (2) TPAN solvatochromic data (black circles) with experimentally measured infrared frequencies and AMOEBA-derived electric fields. DMF, *N*,*N*′-dimethylformamide; DMSO, dimethylsulfoxide; HEX, hexanes; PRD, pyridine; THF, tetrahydrofuran; TOL, toluene. The linear fitting combining the MOF variant data and the TPAN solvatochromic data gives $\bar{\nu} = 0.24F + 2243.2$, with $r^2 = 0.97$, where $\bar{\nu}$ is the wavenumber (cm^{-1}) of the C≡N vibration and F is the magnitude of electric fields (MV cm^{-1}) projected on the C≡N bond axis. The same equation is used to generate the inferred electric field axes on top of the graphics in **a**–**c**. **e**, Fitted Raman spectra for the Ph, CPh, DCPh and AA variants. **f**, Addition of observed Raman shifts and DFT-calculated fields for CPh, DCPh and AA onto the linear VSE plot from aprotic solvents and non-H-bond donors shown in **d** (note the expanded horizontal axis). The vertical deviations from the VSE line are attributed to the H-bond blueshifts.

(TPAN) rather than the less soluble H_3LCN as the model compound for measuring vibrational solvatochromism in aprotic solvents of varying polarity (Supplementary Text 6). The frequency shifts of TPAN in response to solvent polarity were plotted against the solvent electric field magnitudes calculated by molecular dynamics simulations using fixed-charge (GAFF) and polarizable (AMOEBA) force fields (Supplementary Figs. 23–27 and Supplementary Tables 2–4). Compared with fixed-charge force fields, AMOEBA polarizable force fields, which incorporate molecular polarizability, consistently led to solvent electric fields with larger magnitudes, providing a $|\Delta\vec{\mu}|$ of 0.28 cm^{-1}/(MV cm^{-1}). This value is in close agreement with density functional theory (DFT)-based in silico Stark calculations (Supplementary Figs. 28and 29) where a uniform field was applied along the direction of the nitrile in TPAN. These results, together with recent study on nitrile-probed electric fields in photoactive yellow proteins (PYP)[16,17,31], reinforce that polarizability is an indispensable parameter for field estimations of nitriles.

To confirm that TPAN is a valid model compound whose nitrile has similar Stark behaviour as the nitrile probe installed in the MOF using H_3LCN, we applied the geometrical constraints to TPAN that the MOF backbone exerts on the H_4L linker according to the PCN-521 crystal structure (CCDC: DITJOH)[30] (Supplementary Fig. 28) and performed DFT calculations. We found from the in silico Stark calculations that the constraints only slightly change $|\Delta\vec{\mu}|$ (Supplementary Fig. 29). The consistent $|\Delta\vec{\mu}|$ between TPAN and H_3LCN observed from solvatochromism (Supplementary Fig. 23 and Supplementary Tables 5 and 6) corroborates the validity of using TPAN as the model compound. These results confirm the transferability of using the calibration curve obtained from TPAN solutions to infer the magnitude of electric fields inside the MOF (the value of $|\Delta\vec{\mu}|$ was updated later, merging the MOF data with TPAN data into a unifying calibration; Fig. 3).

After calibrating the nitrile probe, we measured the Raman spectra of the MOF variants and found diverse vibrational frequencies for the nitrile (Fig. 3, Supplementary Fig. 30 and Supplementary Table 7). HY, the variant with the simplest and most distant field donor, presents a nitrile frequency of 2,243.2 cm^{-1} (Fig. 3a), essentially the gas-phase frequency, corresponding to an electric field close to zero (0.5 MV cm^{-1}) in the evacuated porous structure. In comparison, hexane, a very non-polar solvent, produces an electric field of −17.1 MV cm^{-1} (polarizable force fields) for the TPAN nitrile (2,239.7 cm^{-1}) (Fig. 3a). To understand the origin of the close-to-zero field in HY, we applied harsh evacuation conditions to induce structural collapse and loss of crystallinity and observed that the nitrile peak broadens and red shifts by 3.4 cm^{-1} (Supplementary Fig. 31), confirming that the MOF porosity is essential

for creating the gas-phase condition for the nitrile. This observation was also noted for the isostructural, Hf-substituted MOF PCN-523 (Supplementary Figs. 32–34). The TFM variant, where the $-CF_3$ group aligns its dipole antiparallel to that of the nitrile, displays a bluer nitrile vibration observed at 2,245.1 cm^{-1}, the first observation of a nitrile in a destabilizing environment (Fig. 3b). The Ph variant—where the stabilizing –Ph field donor is located close to the nitrile—displayed a redshift to 2,240.0 cm^{-1}. With two –F groups added to the –Ph group, the DFPh variant displayed vibrational frequency of 2,239.7 cm^{-1} (Fig. 3c), a small redshift manifesting a weak inductive effect of the –F substituents and a slightly more stabilizing environment for the nitrile.

To understand the observed vibrational shifts, we conducted DFT geometry optimization of the MOF structures using the native PCN-521 crystal structure[30] (CCDC: DITJOH) as the starting model. We then incorporated H_3LCN and the field donors into the structure and located the minima of the potential energy surface. In HY, the installed field donor –H is measured to be 6.23 Å from the N atom in the nitrile based on DFT-optimized structures (Supplementary Fig. 35 and Supplementary Tables 8 and 9), positioning it beyond a range conducive for meaningful H-bond interactions with the nitrile. In Ph and DFPh variants, the *para* H in the –Ph moiety is closer to the N atom in the nitrile (2.45 Å and 2.29 Å, respectively). From these geometries, we generated electrostatic potential (ESP) maps for the interactions between the field donors and the nitrile to estimate the fields (Supplementary Fig. 36). The field calculations from ESP show that the –H in HY produces a negligible field of 0.5 MV cm^{-1} on the nitrile, while the –Ph and –3,5-difluoroPh produces a stabilizing field of –10 MV cm^{-1} and –12.6 MV cm^{-1}, respectively (Supplementary Table 10). The electric field exerted by the $-CF_3$ group is confirmed to be destabilizing and calculated to be +5.5 MV cm^{-1}. In Fig. 3d, we plot the electric field magnitudes of these interactions against the nitrile vibrational frequencies from the Raman measurements.

Overlaying the MOF data points (Raman shifts, DFT-calculated electric fields) with TPAN solvatochromism data points (infrared frequencies, AMOEBA-derived electric fields) reveals a unifying linear correlation with a $|\Delta\vec{f}|$ of 0.24 cm^{-1}/(MV cm^{-1}) and an intercept at 2,243.2 cm^{-1}. The good linearity ($r^2 = 0.97$) indicates that the averaged electric fields produced by bulk solvents and the oriented electric fields exerted by chemical groups installed in the MOF have the same physical foundation, manifesting the power of electric field, a unifying metric for quantifying diverse non-covalent interactions in MOFs and solutions (and proteins) with a common unit. Using the MOF as a platform, we built very low-field chemical environments (HY) approaching that in the gas phase and an unusual destabilizing environment (TFM) for the nitrile, systems unattainable by solvation or protein environments. The unifying linear correlation shown in Fig. 3d also showcases that classical polarizable force fields that use an extensive electrostatic description and quantum mechanically calculated ESP, two different computational methods, now converge into a precise prediction of electric fields. Using the new calibration curve, we add a top axis to Fig. 3a–c to map the readout of the observed nitrile vibrational frequency shifts to the magnitude of electric fields inside the different MOFs.

Anomalous blueshift in frequency due to H bonds formed by protic field donors

With the robust VSE established for aprotic environments, we set out to build and interrogate systems involving H bonds to the nitrile. We installed field donors bearing protic moieties, CPh, DCPh and AA, displaying vibrational frequencies of 2,243.4 cm^{-1}, 2,241.9 cm^{-1} and 2,253.4 cm^{-1}, respectively (Fig. 3e). DFT-based geometry optimization of these structures reveals conformational heterogeneity owing to single-bond rotations within these donors; however, most conformers contain direct H bonds to the nitrile with rather short heavy atom distances (<3 Å) and near head-on angles (>140°) (Supplementary Fig. 35 and Supplementary Tables 9 and 10). The Boltzmann-averaged ESP fields for CPh, DCPh and AA are calculated as –105.0, –123.2 and –96.2 MV cm^{-1} (Supplementary Table 10)—fields of magnitudes that are typically encountered in enzyme active sites and important for catalysis (from –70 MV cm^{-1} to –170 MV cm^{-1})[10,22,23]. In Fig. 3f we add the observed Raman frequencies and calculated fields for CPh, DCPh and AA onto the linear VSE plot from aprotic solvents and non-H-bond donors (Fig. 3d). We attribute the striking deviation from the VSE line to the H-bond blueshifts ($\Delta\bar{\upsilon}_{HB}$), which are 25.6, 28.6 and 33.5 cm^{-1} for CPh, DCPh and AA, respectively (Supplementary Tables 10 and 11). The $\Delta\bar{\upsilon}_{HB}$ in these MOF variants are consistent with predictions from a recent model developed by Kirsh and Kozuch that works on geometric descriptors of electrostatic interactions, with validation through theoretical and experimental data of nitriles embedded in PYP[16,17]. The vibrational Stark effect based on infrared intensities, high-resolution crystal structures and advanced molecular dynamics simulations allow for accurate predictions of $\Delta\bar{\upsilon}_{HB}$ based on H-bond distances (for example, N–O in C≡N···H–O) and H-bond angles (for example, C–N–O in C≡N···H–O) (Supplementary Text 4)[17]. When extrapolated to our MOF variants, where we build H bonds that are shorter and more head-on than those observed in the high-resolution structures of nitrile-substituted PYPs, we observe $\Delta\bar{\upsilon}_{HB}$ larger than protein variants. Thus, the MOF system acts as an excellent experimental platform for building and probing short and head-on H bonds.

We further sought to test whether a weak H bond can be built into the MOF by using –3,5-dinitrophenyl moiety as the field donor. It has a slightly acidic C–H group due to the strong electron-withdrawing nitro substituents, and the DNPh variant exhibits a vibrational frequency of 2,242.0 MV cm^{-1} (Fig. 3c). We calculated the ESP field for DNPh as –24.2 MV cm^{-1}, resulting in a $\Delta\bar{\upsilon}_{HB}$ of 5.6 cm^{-1} (Supplementary Table 11), lying at the smallest end of the $\Delta\bar{\upsilon}_{HB}$ spectrum, consistent with chemical intuition.

Unique solvation under nanoconfinement

We extended the use of the MOF platform to examine unique solvation environments confined in the MOF pore. The nitrile probe is located at the shared window between three octahedral cavities, each of which, with a size of 20.5 × 20.5 × 37.4 Å (ref. 30), can potentially be filled with ~10^2 DMSO molecules. After evacuation, we soaked nitrile-containing MOF crystals in DMSO and measured their Raman spectra. DMSO was selected due to its low vapour pressure and high boiling point, which reduced solvent evaporation during Raman measurements. Upon DMSO solvation, the nitrile in HY showed a redshift by 2.9 cm^{-1} with respect to the solvent-free HY (Fig. 4a), corresponding to a more stabilizing electric field by –12.0 MV cm^{-1} (Supplementary Table 12). Given that the nitrile of TPAN (or H_3LCN) in bulk DMSO experiences an averaged field of –27.4 MV cm^{-1}, the DMSO filled in the MOF pore constitutes a unique solvation environment that produces less than half of the electric field that bulk DMSO does. The solvation environment was also found to be field-donor dependent. The TFM variant displays a redshift by 5.7 cm^{-1} after DMSO solvation, corresponding to an electric field change of –23.5 MV cm^{-1} (Fig. 4b), while the Ph variant exhibits a redshift by only –1.3 cm^{-1}, corresponding to an electric field change of –5.4 MV cm^{-1} (Fig. 4c). This minimal stabilization can be explained by the bulky –Ph group near the nitrile, leaving little space for the solvent to form an effective solvation sphere.

To investigate how solvation perturbs H bonds, we soaked the AA variant in DMSO and observed a dramatic redshift of the nitrile frequency by 14.3 cm^{-1} (Fig. 4d), indicating disappearance of the large H-bond blueshift (33.5 cm^{-1}) characteristic of AA. Assuming no H bond remains, the vibration shift of DMSO-soaked AA can be treated using the purely electrostatic model, resulting in a more destabilizing electric field by 79.2 MV cm^{-1}, a big loss of the stabilizing field due to removal of the strong H bond. The electrostatic effect of solvation in the MOF variants are summarized in Fig. 4e. In addition to the above analysis

https://doi.org/10.1038/s41557-025-01916-7

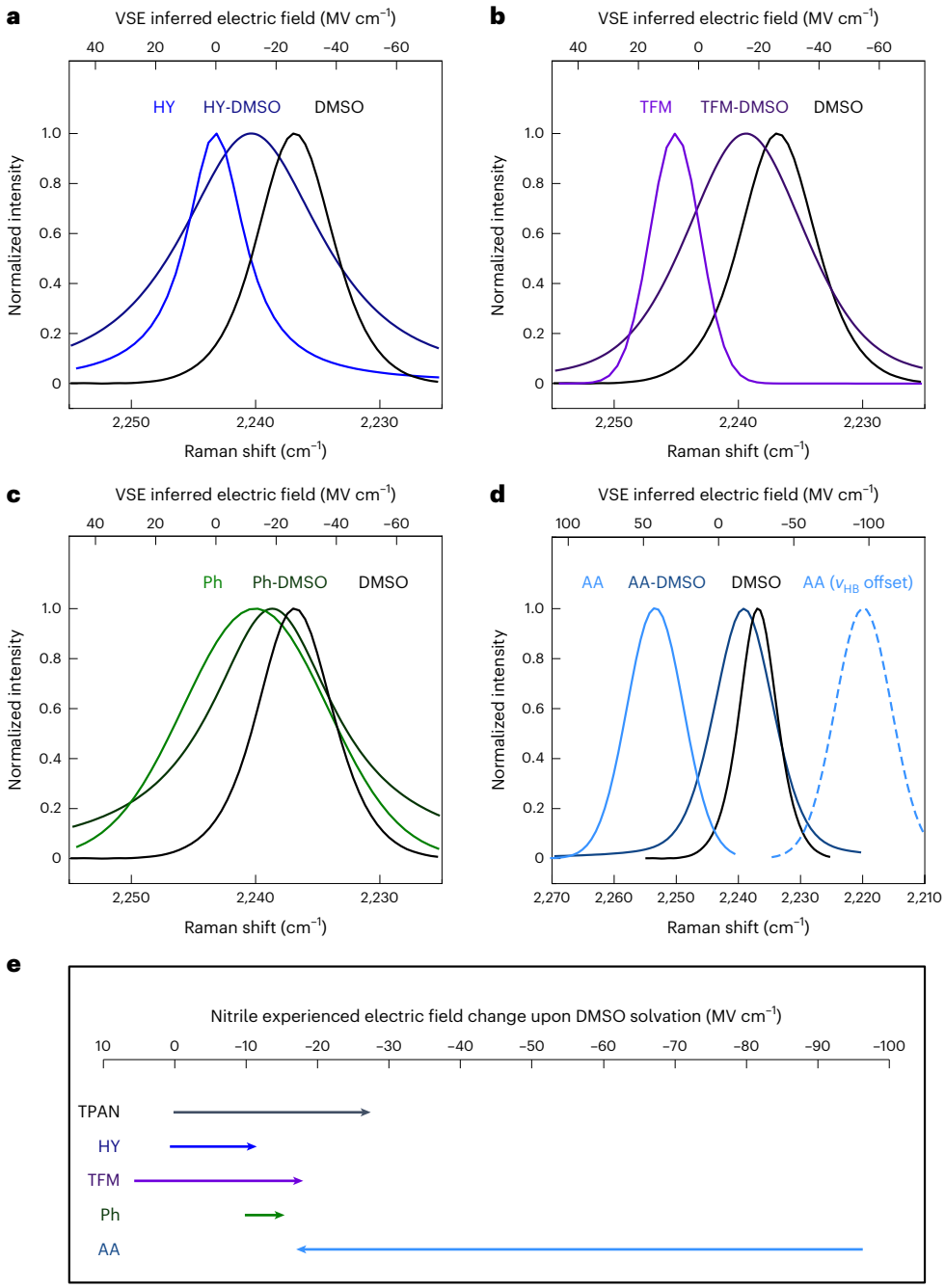

Fig. 4 | Spectroscopic observation and electrostatic quantification of solvation under nanoconfinement. a, Fitted Raman spectra for evacuated HY and the DMSO-solvated HY, overlaid with the infrared spectrum of TPAN in DMSO. **b**, Fitted Raman spectra for the TFM variant and the DMSO-solvated TFM variant, overlaid with the infrared spectrum of TPAN in DMSO. **c**, Fitted Raman spectra for the Ph variant and the DMSO-solvated Ph variant, overlaid with the infrared spectrum of TPAN in DMSO. **d**, Fitted Raman spectra for the AA variant and the DMSO-solvated AA variant, overlaid with the infrared spectrum of TPAN in DMSO. The dashed line plots a hypothetical AA spectrum as if there is no H-bond blueshift (33.5 cm^{-1}). **e**, Changes in the nitrile experienced electric field due to DMSO solvation. The start of the arrows represents the field in the evacuated MOF, while the end of the arrows represents a condition of DMSO-solvated MOF. The electric field for TPAN in DMSO was calculated using AMOEBA force fields. The electric fields for MOF variants in vacuum were calculated based on DFT. The lengths of the arrows, which represents the change in electric field magnitude upon DMSO solvation, was obtained from the observed frequency shifts and the corresponding VSE inferred electric fields shown in **a**–**d**.

of the change in field magnitude upon DMSO solvation (Fig. 4e, arrow length), the final total electric field (Fig. 4e, arrow end) provides a quantitative description of the solvent-filled MOF pore as a whole. The magnitude of electric fields produced by the DMSO-filled MOF pores sit in a narrow range from −12 to −18 MV cm^{-1}, regardless of the pre-installed electric field donors, manifesting the common effect of field screening by solvent. These fields are consistently smaller than that produced by the bulk DMSO solvation (−27.4 MV cm^{-1}), indicating that solvation under nanoconfinement provides unique chemical environments that are distinct themselves from solvation in bulk. Similar anomalous solvation was also observed for other solvents confined in the MOF nanopore (Supplementary Text 7 and Supplementary Fig. 37). Electric fields in confined environments may be related to the catalysis observed inside MOF pores and other supramolecular cages, and our

results indicate that to fully take advantage of the electric fields produced by the confined environment, one has to minimize the effect of field screening by the solvent, possibly by tailoring the pore size or installing functional groups to preclude solvent molecules or specifically organize solvent molecules.

Conclusions

We have shown that the PCN-521 MOF framework can be used as a general platform to create a series of non-covalent interactions using a modular molecular approach. The synthesized non-covalent interactions were interrogated by Raman spectroscopy and interpreted within the framework of the vibrational Stark effect giving the electric fields a donor exerts onto an acceptor. We found that the electric fields associated with non-covalent interactions are highly diverse, from being as destabilizing as +6 MV cm^{-1} (TFM) to being as stabilizing as −123 MV cm^{-1} (DCPh). The electric field provides an absolute, quantitative metric enabling broad comparisons across various chemical groups in terms of their electrostatic properties. Using the platform, we identified electric fields (HY) as weak as those in gas phase, positive fields (TFM) associated with destabilizing environment and H bonds (CPh, DCPh and AA) that are stronger than those in certain proteins. We further studied the non-covalent interactions involved in solvation by utilizing the microporous structure of the MOF to create solvent organizations that are inaccessible by the bulk. These results and analysis not only address fundamental questions about elementary interactions in chemistry, biology and material sciences, but also provide useful tools for molecular design and engineering, for example, the creation of novel catalysts using the principle of electrostatic catalysis.

Online content

Any methods, additional references, Nature Portfolio reporting summaries, source data, extended data, supplementary information, acknowledgements, peer review information; details of author contributions and competing interests; and statements of data and code availability are available at https://doi.org/10.1038/s41557-025-01916-7.

References

1. Furukawa, H., Cordova, K. E., O'Keeffe, M. & Yaghi, O. M. The chemistry and applications of metal–organic frameworks. *Science* **341**, 1230444 (2013).
2. Li, H., Eddaoudi, M., O'Keeffe, M. & Yaghi, O. M. Design and synthesis of an exceptionally stable and highly porous metal–organic framework. *Nature* **402**, 276–279 (1999).
3. Freund, R. et al. 25 years of reticular chemistry. *Angew. Chem. Int. Ed.* **60**, 23946–23974 (2021).
4. Wang, Y., Liu, Q., Zhang, Q., Peng, B. & Deng, H. X. Molecular vise approach to create metal-binding sites in MOFs and detection of biomarkers. *Angew. Chem. Int. Ed.* **57**, 7120–7125 (2018).
5. Yan, W. et al. Molecular vises for precisely positioning ligands near catalytic metal centers in metal–organic frameworks. *J. Am. Chem. Soc.* **142**, 16182–16187 (2020).
6. Chen, W. H. et al. Precise distance control and functionality adjustment of frustrated Lewis pairs in metal–organic frameworks. *J. Am. Chem. Soc.* **146**, 12215–12224 (2024).
7. Chattopadhyay, A. & Boxer, S. G. Vibrational Stark-effect spectroscopy. *J. Am. Chem. Soc.* **117**, 1449–1450 (1995).
8. Fried, S. D. & Boxer, S. G. Measuring electric fields and noncovalent interactions using the vibrational Stark effect. *Acc. Chem. Res.* **48**, 998–1006 (2015).
9. Park, E. S., Andrews, S. S., Hu, R. B. & Boxer, S. G. Vibrational stark spectroscopy in proteins: a probe and calibration for electrostatic fields. *J. Phys. Chem. B* **103**, 9813–9817 (1999).
10. Fried, S. D., Bagchi, S. & Boxer, S. G. Extreme electric fields power catalysis in the active site of ketosteroid isomerase. *Science* **346**, 1510–1514 (2014).
11. Fried, S. D., Bagchi, S. & Boxer, S. G. Measuring electrostatic fields in both hydrogen-bonding and non-hydrogen-bonding environments using carbonyl vibrational probes. *J. Am. Chem. Soc.* **135**, 11181–11192 (2013).
12. Suydam, I. T., Snow, C. D., Pande, V. S. & Boxer, S. G. Electric fields at the active site of an enzyme: direct comparison of experiment with theory. *Science* **313**, 200–204 (2006).
13. Slocum, J. D. & Webb, L. J. Measuring electric fields in biological matter using the vibrational Stark effect of nitrile probes. *Annu. Rev. Phys. Chem.* **69**, 253–271 (2018).
14. Fafarman, A. T. & Boxer, S. G. Nitrile bonds as infrared probes of electrostatics in ribonuclease S. *J. Phys. Chem. B* **114**, 13536–13544 (2010).
15. Yang, Y. Y., Feng, R. R. & Gai, F. 4-Cyanotryptophan as a sensitive fluorescence probe of local electric field of proteins. *J. Phys. Chem. B* **127**, 514–519 (2023).
16. Weaver, J. B., Kozuch, J., Kirsh, J. M. & Boxer, S. G. Nitrile infrared intensities characterize electric fields and hydrogen bonding in protic, aprotic, and protein environments. *J. Am. Chem. Soc.* **144**, 7562–7567 (2022).
17. Kirsh, J. M. & Kozuch, J. Hydrogen bond blueshifts in nitrile vibrational spectra are dictated by hydrogen bond geometry and dynamics. *JACS Au* **4**, 4844–4855 (2024).
18. Yang, Y. Y., Liu, J. S., Feng, R. R., Zhang, W. K. & Gai, F. C≡N stretching frequency as a convenient reporter of charge separation in molecular systems. *J. Phys. Chem. B* **127**, 6999–7003 (2023).
19. Du, J. J., Wang, H. M. & Wei, L. Bringing vibrational imaging to chemical biology with molecular probes. *ACS Chem. Biol.* **17**, 1621–1637 (2022).
20. Schneider, S. H., Kozuch, J. & Boxer, S. G. The interplay of electrostatics and chemical positioning in the evolution of antibiotic resistance in TEM β-lactamases. *ACS Cent. Sci* **7**, 1996–2008 (2021).
21. Ji, Z. et al. Protein electric fields enable faster and longer-lasting covalent inhibition of β-lactamases. *J. Am. Chem. Soc.* **144**, 20947–20954 (2022).
22. Ji, Z. & Boxer, S. G. β-Lactamases evolve against antibiotics by acquiring large active-site electric fields. *J. Am. Chem. Soc.* **144**, 22289–22294 (2022).
23. Zheng, C., Ji, Z., Mathews, I. I. & Boxer, S. G. Enhanced active-site electric field accelerates enzyme catalysis. *Nat. Chem.* **15**, 1715–1721 (2023).
24. Shrestha, R., Cardenas, A. E., Elber, R. & Webb, L. J. Measurement of the membrane dipole electric field in DMPC vesicles using vibrational shifts of *p*-cyanophenylalanine and molecular dynamics simulations. *J. Phys. Chem. B* **119**, 2869–2876 (2015).
25. Hu, W. H. & Webb, L. J. Direct measurement of the membrane dipole field in bicelles using vibrational Stark effect spectroscopy. *J. Phys. Chem. Lett.* **2**, 1925–1930 (2011).
26. Bagchi, S., Fried, S. D. & Boxer, S. G. A solvatochromic model calibrates nitriles' vibrational frequencies to electrostatic fields. *J. Am. Chem. Soc.* **134**, 10373–10376 (2012).
27. Zheng, C. et al. A two-directional vibrational probe reveals different electric field orientations in solution and an enzyme active site. *Nat. Chem.* **14**, 891–897 (2022).
28. Sarkar, S., Maitra, A., Banerjee, S., Thoi, V. S. & Dawlaty, J. M. Electric fields at metal–surfactant interfaces: a combined vibrational spectroscopy and capacitance study. *J. Phys. Chem. B* **124**, 1311–1321 (2020).
29. Delley, M. F., Nichols, E. M. & Mayer, J. M. Electrolyte cation effects on interfacial acidity and electric fields. *J. Phys. Chem. C* **126**, 8477–8488 (2022).

30. Zhang, M. W. et al. Symmetry-guided synthesis of highly porous metal–organic frameworks with fluorite topology. *Angew. Chem. Int. Ed.* **53**, 815–818 (2014).
31. Schneider, S. H. & Boxer, S. G. Vibrational Stark effects of carbonyl probes applied to reinterpret IR and Raman data for enzyme inhibitors in terms of electric fields at the active site. *J. Phys. Chem. B* **120**, 9672–9684 (2016).

Data availability

All data supporting the findings of this study are available in the Article and its Supplementary Information. Source data are provided with this paper.

Acknowledgements

This work was supported by the International Human Frontier Science Program Organization (no. RGP0047/2022 to S.W. and S.G.B.) and, in part, by NIH grant (no. GM118044 to S.G.B.). Part of this work was performed at the Stanford Nano Shared Facilities, supported by the National Science Foundation under award ECCS-2026822.We would also acknowledge the use of services from the Stanford Sherlock HPC facility. J.A. thanks the Ministerio de Ciencia e Innovación and the European Union–NextGenerationEU for a Juan de la Cierva Formación (no. FJC2021-048154-I to J.A.) research contract. F.P. and G.J.-O. thank MCIN/AEI (grant nos RYC2022-036457-I and EUR2023-143462 to F.P. and PID2021-125946OB-I00 and PDC2022-133725-C22 to G.J.-O.). We thank J. Kirsh, J. Kozuch, S. Fried and M. Asadi for discussions.

Author contributions

Z.J., S.W. and S.G.B. designed the research. Z.J. and S.M. performed the experiments and data analysis, including MOF synthesis, PXRD measurements, NMR spectroscopy, Raman spectroscopy and infrared spectroscopy. S.M., F.P. and G.J.-O. performed the computation. A.S. and J.A. synthesized the H_3LCN linker and supported the MOF synthesis. Z.J., S.M., J.A., S.W. and S.G.B discussed the results. Z.J., S.M., S.W. and S.G.B wrote the paper.

Competing interests

The authors declare no competing interests.

Additional information

Supplementary information The online version contains supplementary material available at https://doi.org/10.1038/s41557-025-01916-7.

Correspondence and requests for materials should be addressed to Zhe Ji, Stefan Wuttke or Steven G. Boxer.

Peer review information *Nature Chemistry* thanks the anonymous reviewers for their contribution to the peer review of this work.